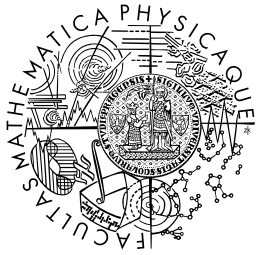

FACULTY
OF MATHEMATICS
AND PHYSICS
Charles University

BACHELOR THESIS

Jakub Überlauer

Chromospheric activity in K giant stars

Astronomical Institute of Charles University

Supervisor of the bachelor thesis: Mgr. Marie Karjalainen, Ph.D.
Study programme: Physics
Study branch: FP

Prague 2023

I declare that I carried out this bachelor thesis independently, and only with the cited sources, literature and other professional sources. It has not been used to obtain another or the same degree.

I understand that my work relates to the rights and obligations under the Act No. 121/2000 Sb., the Copyright Act, as amended, in particular the fact that the Charles University has the right to conclude a license agreement on the use of this work as a school work pursuant to Section 60 subsection 1 of the Copyright Act.

In ..... date ....

Author's signature

I would like to thank my family and friends for supporting me during my studies and my supervisor, Mgr. Marie Karjalainen, Ph.D., for the amazing opportunity to work on an article and all the help with this thesis.

Title: Chromospheric activity in K giant stars

Author: Jakub Überlauer

Institute: Astronomical Institute of Charles University

Supervisor: Mgr. Marie Karjalainen, Ph.D., Astronomical Institute of Czech Academy of Sciences

Abstract: In this bachelor thesis, we analyze chromospheric activity of two K giant stars, HD 187878 and KIC 3526061, which have been monitored for the past 10 years and have shown variations in their radial velocities that could be caused either by a star's companion, a yet to be discovered type of stellar oscillations or a modulation due to stellar surface features as a result of stellar activity. We explain the physics and theory behind the measurements and we apply it directly to observed data. After the procession of data, we look for periodicities and discuss the results.

Keywords: chromospheric activity, K giant stars, spectroscopy, Calcium lines, exoplanets

Contents

Introduction **3**

1 Stellar properties and activity **5**
1.1 Spectral types . . . 5
1.2 Stellar structure . . . 6
1.3 Red giants . . . 7

2 Exoplanets and their detection techniques **9**
2.1 Direct imaging . . . 9
2.2 Transit photometry . . . 9
2.3 Gravitational microlensing . . . 10
2.4 Timing methods . . . 10
2.4.1 Pulsar timing . . . 11
2.4.2 Transit timing . . . 11
2.5 Radial velocity . . . 11

3 Spectral analysis **13**
3.1 Spectra . . . 13
3.2 Equivalent width measurements . . . 14
3.3 Chromospheric activity measurements . . . 15

4 Software overview **17**
4.1 IRAF . . . 17
4.2 Period04 . . . 18

5 Results **19**
5.1 HD 187878 . . . 19
5.2 KIC 3526061 . . . 21

Conclusion **23**

Bibliography **25**

List of Figures **27**

List of Tables **29**

Introduction

Ever since we as humans started wandering around the Earth, we have had the same philosophical struggles. Looking up the night sky at all the stars scattered throughout it, we have always wondered if there is such a place as our home somewhere far far away. The heliocentric revolution has sparked an idea of such worlds orbiting distant stars, and since the first ever confirmed detection of a planet orbiting a main sequence star other than Sun in 1995, the detection techniques of exoplanets have immensely improved and the hunt for exoplanets has begun.

Out of all the possibilities, Doppler spectroscopy and transit photometry have proven themselves to be the most efficient so far, although they are not suitable for every spectral type. They are both very reliable methods when it comes to stars of a mass approximately less than 1 solar mass. However, detecting a planet transit for a star of an intermediate mass (1.2-2 solar masses) is proven to be more difficult than for a star of a lower mass, due to the simple fact of heavier stars having bigger stellar radii, thus transit signals being weaker and harder to detect. Detecting a stellar companion of an intermediate-mass main sequence star via the Doppler spectroscopy method is also difficult, given that main sequence stars are very hot, therefore they do not exhibit enough spectral lines for radial velocity measurements. Main sequence stars also show a significant amount of rotation around their axes, which results into broadening and shallowing of the spectral lines, making them unsuitable for a precise measurement.

Nonetheless, using the Doppler method on intermediate-mass stars evolved into giants brings positive results. These giant stars reach lower surface temperatures, resulting in more atomic lines and molecular bands in their spectra, and usually have slower rotation rates, resulting in lines being narrower and deeper. With such spectra, radial velocity measurements for these giants are way more precise, resulting in precision of several $\mathrm{m\,s^{-1}}$ rather than tens of $\mathrm{m\,s^{-1}}$ for their main sequence progenitors.

In this thesis, we take a look at two K giant stars, HD 187878 and KIC 3526061. These were two planet candidate stars which have been monitored for over the past 10 years and have exhibited a behavior that could be explained either by an orbiting companion, a yet to be discovered type of stellar oscillation, or stellar activity. First, we explain the theory behind such stars, go through various exoplanetary detection techniques and take a closer look at the theory behind Doppler spectroscopy. Then we measure equivalent widths of Calcium spectral lines as indicators of the chromospheric activity, and look for periodicities in our measurements with dedicated software. We use data observed by the HERMES echelle spectrograph at the Mercator telescope. Based on the results, we finally conclude about a potential planetary or stellar companions and their properties.

1. Stellar properties and activity

Given the different times, locations and conditions of their formation, stars are immensely diverse objects. To better understand their life cycles and properties, many different categorizations have been created based on the modern-day photometric and spectrometric astronomical measurements. The creation of one of the most recognized diagrams in astrophysics was carried out in the beginning of the 20th century by E. Hertzsprung and H. N. Russell. The Hertzsprung-Russell diagram plots the spectral type, surface temperature or color index of stars against their luminosity (Hanslmeier [2020]), as shown in Fig. 1.1. In other words, based on the position of the star on the diagram, one can obtain information about the star's temperature, mass, age and luminosity.

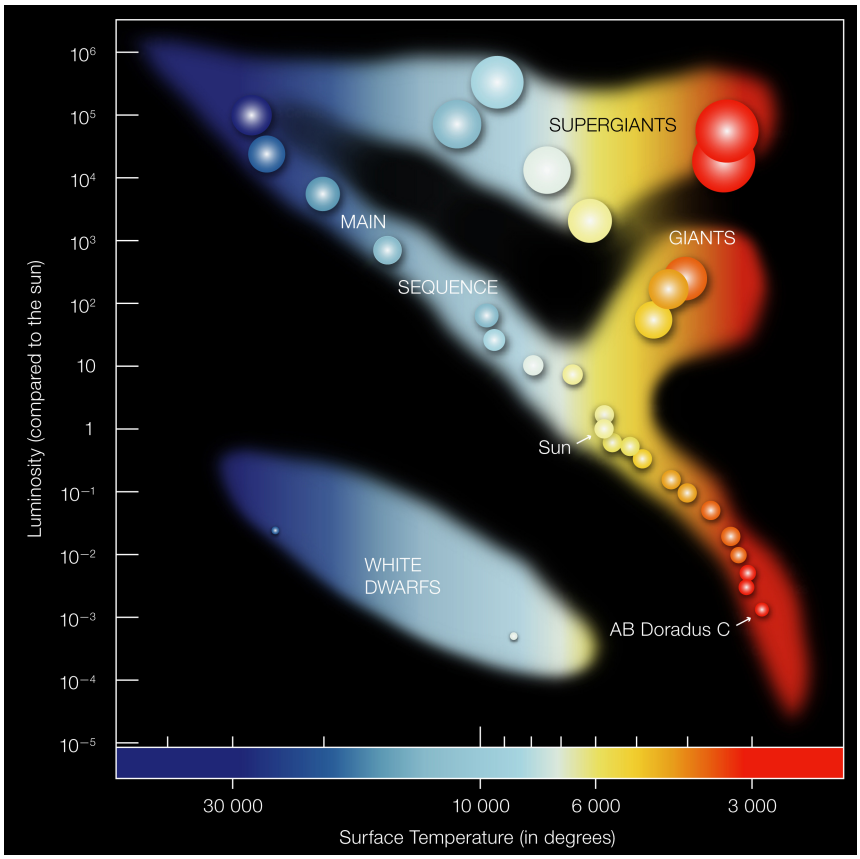

Figure 1.1: The Hertzsprung-Russell diagram. ESO

1.1 Spectral types

The modern classification of stars according to their spectra is represented by the sequence O-B-A-F-G-K-M, where O stars (blue-violet) are the hottest ones, with their surface temperatures peaking at over 30000 K, and M stars (red-orange) being the coolest ones, with surface temperatures at around 3000 K. Cooler stars' spectra showcase a variety of spectral lines of heavier elements, whereas hotter stars of O spectral type mainly feature ionized He spectral lines. As a result,

cooler stars are preferred in spectrometric measurements due to more accurate radial velocity measurements coming from more spectral lines.

The relation between a star's temperature, T, and color can be derived from the *Wien's law* (with the assumption of the star radiation being like that of a black body):

$$T\lambda_{max} = \text{const} \tag{1.1}$$

where λ_{max} represents the wavelength where the maximum emission occurs in the spectrum. From this equation, it is obvious that hot stars emit more radiation at shorter wavelengths (going towards blue), while cool stars emit more at longer ones (going towards red).

The relation between a star's effective temperature, T_{eff}, and its total radiative output is characterized by the *Stefan-Boltzmann law*:

$$E = \sigma T_{eff}^4 \tag{1.2}$$

where $\sigma = 5.67 \times 10^{-8}\text{Wm}^{-2}\text{K}^{-4}$ and the stellar effective temperature gives an estimate of a stellar surface temperature. Therefore, the hotter the star, the bigger the total energy output.

Given the logical conclusion of a larger surface allowing to emit more radiation than smaller surfaces, it is natural that bigger stars have a higher luminosity. Assuming a star's surface area is a sphere with the area of $4\pi R^2$, the luminosity of the star is calculated as:

$$L = 4\pi R^2 \sigma T_{eff}^4 \tag{1.3}$$

1.2 Stellar structure

To better understand the terms we will talk about and use later, it is useful to mention the general structure of the stars and the processes that take place inside of them. It is important to acknowledge the fact that the stars are self-gravitating due to their immense mass and the fact that the structure of a star obeys a set of equations. All the processes inside exist in an equilibrium, meaning shifts in temperatures and composition provoke changes to maintain it.

At the center, we have the star's core. In younger main-sequence stars, the core is where the fusion of hydrogen into helium takes place. The nuclear fusion is the energy source of a star. With time, the core runs out of fuel, having fused all of its hydrogen into helium and turning itself into an inert environment until it reaches temperatures hot enough to start fusing helium into carbon in the three-alpha process. Energy gets transferred to the outer layers via the convection and/or radiative zone (or, in case of white dwarfs, via the thermal conduction), with the conduction zone, in general, being the dominant mode of transport of the energy. The mode of transport depends on the mass of the star, as illustrated in Fig. 1.2.

The outer shell of a star is denominated photosphere. Its name originates from Ancient Greek and it comes from it being the layer that emits the light. Above it, we have the star's atmosphere known as the chromosphere. As the name of this thesis suggests, this is the layer we are interested in and will analyze later.

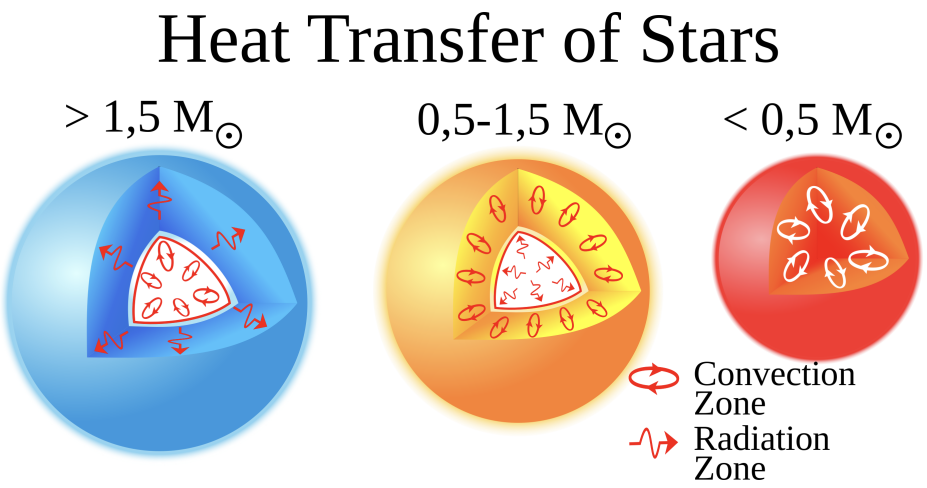

Figure 1.2: Heat transfer of stars depending on their mass. Wikipedia

The chromosphere is further away from the star's core and is less dense than the photosphere, thus its temperature is lower. This is the place where the spectral absorption lines are created, by the elements which absorb a stellar radiation with certain energies, depending on the composition of the chromosphere and properties of the star itself (age, spectral type etc.). We use these absorption lines to perform spectral analysis described later in this work.

1.3 Red giants

In general, red giants are stars of approximately 0.3 - 8 solar masses with surface temperatures around 5000 K. This term includes mainly the spectral types K and M. Red giants are older stars which evolved from main-sequence stars when their cores ran out of hydrogen supply. When this happens, the core starts to collapse, and the layer around it reaches a temperature high enough to begin to fuse hydrogen contained in it. At the same time, the heat causes the expansion of outer stellar layers into space, including their outer atmospheres, hence the large radii of red giants.

Due to this expansion into space, the temperature of outer layers is lower, which is responsible for their appearance, since their color ranges from yellow-white to reddish-orange. Later evolutionary stages of red giants involve Helium fusion in the core and in the outer layer around it, while the stellar radius continues to increase for most of the time. Finally, the process is terminated by that a giant star starts to lose material until only the degenerated core remains. At the beginning, the core is still extremely hot and illuminates the surrounding material that has been lost. This is called a planetary nebula. The core gradually cools down and the planetary nebula gets dispersed into the space, and finally only a white dwarf remains.

2. Exoplanets and their detection techniques

As the term extrasolar planet suggests, it is by a definition a planet orbiting a star different than the Sun. The first confirmation of detection of such a body occurred on 9 January 1992, with the discovery of the planetary system around the pulsar PSR B1257+12 by Aleksander Wolszczan and Dale Frail (Wolszczan [1994]). The first discovery of an exoplanet orbiting a main sequence star was made on 6 October 1995 by Michel Mayor and Didier Queloz (Mayor and Queloz [1995]). This discovery of 51 Pegasi b was awarded by the Nobel Prize in Physics in 2019. According to NASA, as of 10 April 2023, 5332 exoplanets have been confirmed, with NASA's Kepler Telescope discovering 2709, K2 discovering 544 and TESS discovering 329 of them[1].

2.1 Direct imaging

There are various methods of detecting extrasolar planets, but only several are being used with good results. The direct method of detection is called direct imaging. A planet of a big enough radius located far enough from the parent star can be directly detected and imaged using special instruments. However, this method poses a technological challenge, since it is required to block the parent star light while still being able to capture the light reflected by the planet, keeping in mind the small ratio of the intensity of light reflected by the planet and the light emitted by its parent star.

2.2 Transit photometry

Transit photometry is a widely used method of detection of exoplanets. It is based on the analysis of the change of star's magnitude when a planet crosses in front of it (see Fig. 2.1). NASA's Kepler Telescope uses this method.

It can also be used to determine the composition of the observed planet's atmosphere using spectral analysis of the light during the planet's transit, as the light emitted by the parent star passes through the planet's atmosphere and interacts with it.

Although it is a very popular method, there are two big disadvantages to it. To discover a planet using this method, it is required that at least a partial transit is observable from our Solar System, thus only the planets with a correct orientation of their orbital planes can be detected. The probability of a transit being observable from the astronomers' vantage point is defined as the ratio of the star's diameter to the planetary orbit's semi-major axis, ergo it decreases for large orbits. The second disadvantage of this method is the high rate of false detections. Many exoplanetary candidates are analyzed via other methods to confirm their exoplanetary status.

[1] exoplanetarchive.ipac.caltech.edu, cited 10 April 2023

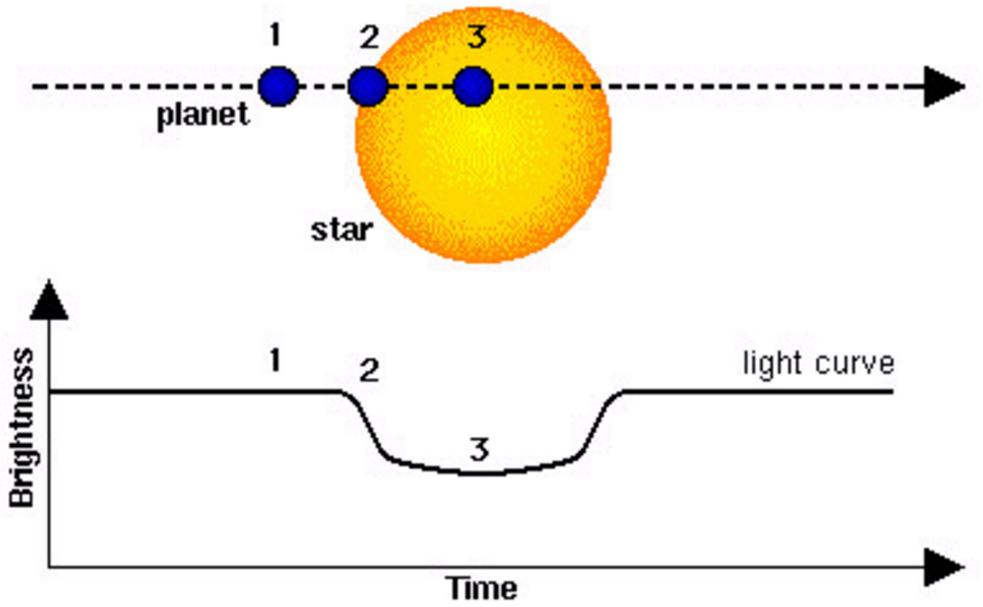

Figure 2.1: Illustration of changes of a star's brightness during a planetary transit. ESA

2.3 Gravitational microlensing

Gravitational microlensing is another method used in exoplanetary research. Using the principles of the theory of relativity, gravitational microlensing method is based on the light-bending effects of gravity. When an exoplanetary candidate star (lens star) passes in front of (or close enough to) another star (source star), the light emitted by the source star is bent. If the lensed star has an exoplanet, the planet contributes to the light's curvature with its own gravity, alternating the expected curvature.

The disadvantage of this method is mainly the fact that the correct alignment events last for a short period of time, usually for days or weeks, and, due to the improbable nature of these alignments happening frequently, it is required to monitor multiple stars for it to be effective and give positive results.

Another big disadvantage of this method is the simple fact that lensing events cannot be observed again. However, gravitational microlensing is a very strong tool for finding exoplanets around stars positioned in front of the galaxy's center relative to astronomers' vantage point, since it has a large population of stars, thus the probability of the correct alignments is much higher.

2.4 Timing methods

There are also various timing methods which are more complicated and specialized in their nature, nonetheless they have proven to be effective in their realms.

2.4.1 Pulsar timing

Pulsar timing was used by Wolszczan and Frail in the 1992's discovery of the first exoplanetary system orbiting the pulsar PSR B1257+12 (Wolszczan [1994]). Pulsars are a type of a neutron star (extremely dense remnant of a star) emitting regular radio waves due to the very fast rotation around their axes. Since planets and other bodies don't orbit around the parent star's center, but rather the whole system orbits its common barycenter, so do pulsars. The movement of pulsars with bodies orbiting them can be traced by pulse-timing, therefore allowing calculations of the parameters of the bodies depending on pulsar's small orbit around the barycenter. Although it is a very specific method, it has been proven to be the most precise, allowing planets with mass of approximately one tenth of the Earth's to be detected.

2.4.2 Transit timing

Transit timing and transit duration variations are used in multi-planetary systems. Both methods are based on the variability of periodical transits. Planets in such systems influence each other's motion with their own gravity fields, which causes them to accelerate or decelerate in some parts of their orbits. Data from these measurements are then used to model systems, including the number of planets, their orbits, and their respective masses.

2.5 Radial velocity

One of the most used methods of detecting exoplanets and other bodies orbiting other stars is the radial velocity method, also known as Doppler spectroscopy. The movement of any object can be decomposed into two components, one being the projection of the object's movement onto the line of sight of the observer and the other one being perpendicular. The line of sight component of the object's velocity is referred to as the radial velocity, the perpendicular component is respectively the tangential (or transverse) velocity. For these measurements, only radial component of the movement is useful, as it is the only one that allows the observer to detect changes in wavelengths.

As it was mentioned in previous paragraphs, all bodies in planetary systems orbit a common center of gravity denominated the barycenter. Given that the electromagnetic radiation travels through space with a constant velocity, the movement of the parent star influences the wavelength of its emitted radiation according to the Doppler's effect. The ratio of the observed and the real wavelength is given as:

$$\frac{\lambda}{\lambda_0} = \frac{1 + \frac{v}{c}\cos\theta}{\sqrt{1 - \frac{v^2}{c^2}}}, \tag{2.1}$$

where λ_0 is the emitted wavelength, λ is the observed wavelength, θ is the angular deviation of the movement of the body, v is the velocity of the body and c is the speed of light. For small speeds $v \ll c$ we denote the radial velocity v_r as $v_r = v\cos\theta$. We now have:

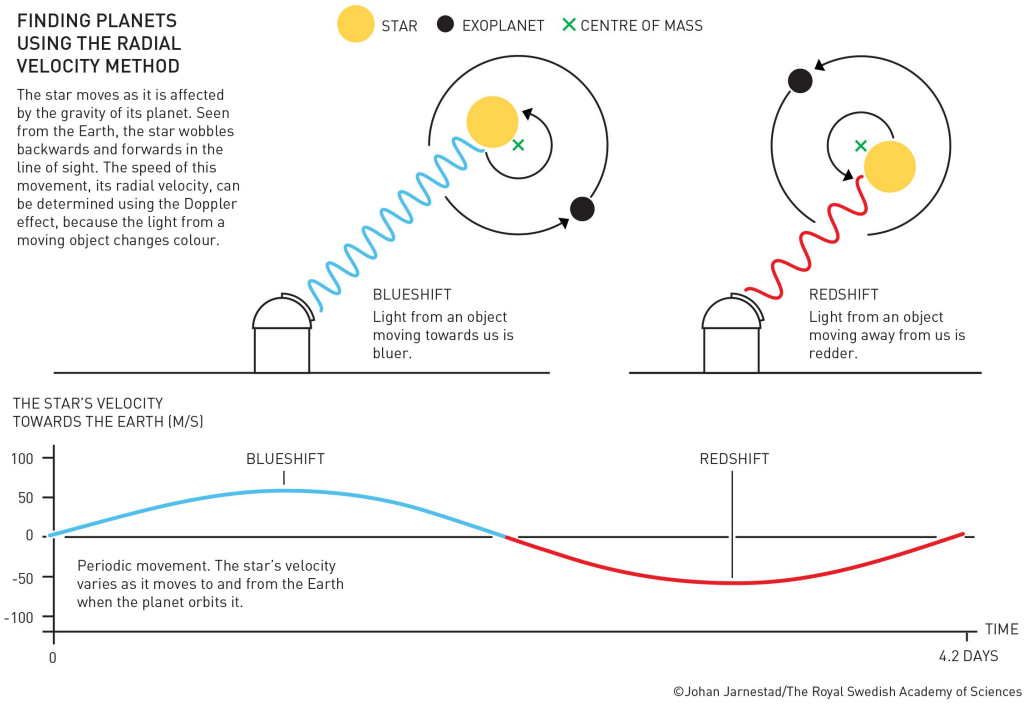

Figure 2.2: A visual depiction of the Doppler effect caused by the movement of a star around the system's barycenter. The Royal Swedish Academy of Science

$$\frac{\lambda}{\lambda_0} = 1 + \frac{v_r}{c}. \tag{2.2}$$

Out of this equation, we can calculate the radial velocity as:

$$v_r = c\frac{\lambda - \lambda_0}{\lambda_0}. \tag{2.3}$$

When a star is moving closer relatively to the observer (in our coordinate system $v_r < 0$), the wavelength of the emitted radiation is shortened ($\lambda < \lambda_0$). Analogically, the wavelength elongates ($\lambda > \lambda_0$) while moving further from the observer ($v_r > 0$). These shifts in wavelength (and thus frequencies) are labeled as the red and blue shift, stemming from the properties of the electromagnetic radiation in the visible light spectrum – red light has the longest wavelengths, blue light has them shorter (see Fig. 2.2).

Stars emit a wide spectrum containing useful information. All elements have their individual emission and absorption spectra; hence it is possible to analyze the star's compounds by breaking down the spectrum of the emitted light using the empirically known values of the spectral lines. Depending on the type of the observed star, one can use the spectral lines of expected elements to determine the shift of the spectrum. With long enough observations of the candidate star, data can be fitted, and periodicities can be searched for. This method has been proven useful not only to detect exoplanets, but other bodies, for example, brown dwarfs, white dwarfs, binary stars or multiple stars, given the fact that for such great distances, it is almost impossible to distinguish multiple star systems purely by direct imaging. We used this method to analyze radial velocities of HD 187878 and KIC 3526061.

3. Spectral analysis

Modern astronomy measurements are in majority based on spectrometry. The emitted radiation contains a variety of useful information from which other data can be extracted. These spectrometric measurements are based on the properties of stellar spectra.

3.1 Spectra

The observed radiation is broken up into components through diffraction. A broken down spectrum can be either a continuous, an absorption or an emission one, depending on the properties of the environment the emitted radiation passes through (see Fig. 3.1).

A continuous thermal spectrum is a complete continuum of the emitted light. An emission line spectrum is observed after the diffraction of the light emitted by a hot gas. It is characterized by a set of separate lines (in case of atoms) or short bands of light (in case of molecules). An absorption line spectrum is observed when light emitted by a hot gas passes through a layer of cooler gas. Its appearance is characterized by missing emission lines in a continuous spectrum. The wavelength of the emission/absorption lines is based on the properties of individual elements contained in the gas.

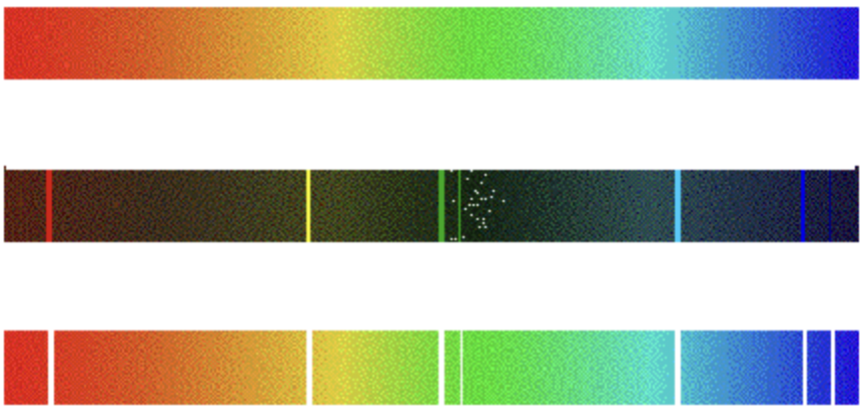

Figure 3.1: A continuous, an emission and an absorption spectrum. University of Rochester

We use absorption line spectra to measure chromospheric activity. The chromosphere is by definition the atmosphere of a star, therefore its temperature is lower than that of the star's interior. The cooler gas in the chromosphere absorbs a portion of the light emitted from inside a star which we observe in form of absorption lines. The temperature and composition of the chromosphere vary depending on the stellar type.

Every element (and molecule) has its own unique set of spectral lines caused by the interaction between a quantum system and a photon. Being unique, the sets allow us to distinguish between the elements.

As mentioned above, the composition and the temperature of the chromosphere depend on the stellar type. In Fig. 3.2), the black-body radiation model was used to calculate the wavelength and intensity of the emitted radiation.

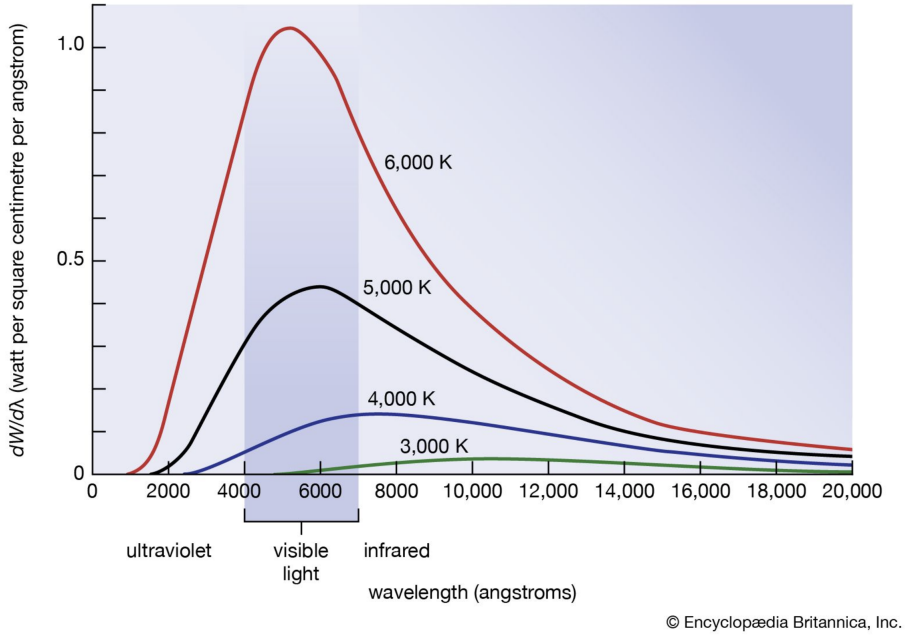

Figure 3.2: The black-body radiation model. Encyclopaedia Britannica.

The radiation is (of course) polychromatic, meaning each wavelength is emitted at a different rate, hence it has its own intensity. Combining this with the composition variety of different chromospheres, we see that depending on the stellar type we observe spectral lines of different compounds. The temperature of the chromosphere of a K giant star is set between 4000 and 5250 K, while the most distinguishable features of its spectrum are Ca^+ and Fe lines with strong presence of CH and CN molecules.

3.2 Equivalent width measurements

The measurement of equivalent widths (EQW) is one of the strongest tools for analyzing the effects of temperature and gravity on absorption features of stellar atmospheres (Stetson and Pancino [2008]). The EQW is by definition the width of a rectangular area of the same size as the area of the observed absorption line (starting from the continuum level (I_C) down to the specific flux at the line center (I_0)), as depicted in the Fig. 3.3. The rectangular area is of height I_C.

The EQW of an isolated spectral line in a discretely-sampled spectrum is defined as:

$$EQW = \Delta\lambda \sum_i \frac{I_{C_i} - I_i}{I_{C_i}} \tag{3.1}$$

where $\Delta\lambda$ is the constant pixel size, I_{C_i} is the continuum level at the wavelength of the i-th pixel, and I_i is the actual flux received by the i-th pixel.

However, when handling real-life observed spectral data, the profile of a spectral line is affected by noise, spectral defects, other lines and/or the movement of

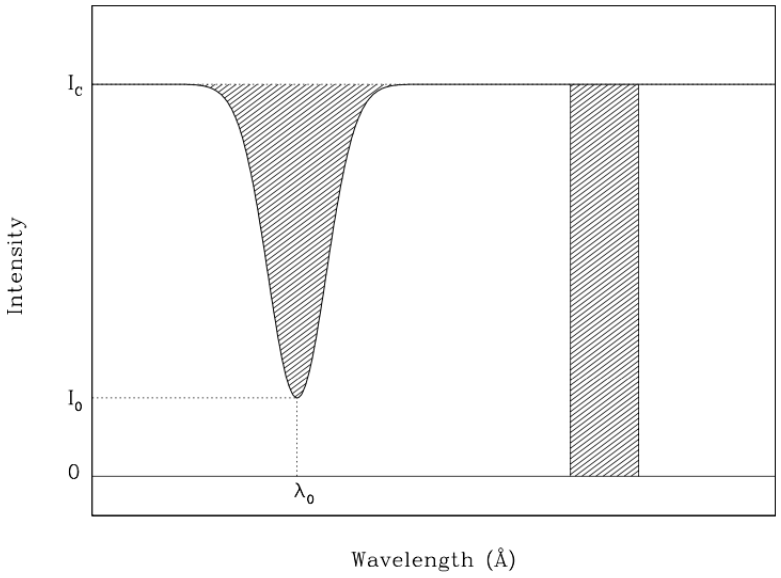

Figure 3.3: Visual representation of the EQW definition. Stetson and Pancino [2008]

the star, both rotation around its axis and rotation around the barycenter of the system. The deformation of a spectral line can be resolved by fitting a Gaussian profile over the line, often done by a numerical fit of a Gaussian-shaped function $g(\lambda)$ defined as:

$$g(\lambda) = Ae^{(\lambda-\lambda_0)^2/2\sigma^2}, A > 0 \tag{3.2}$$

The specific flux by the i-th pixel is then defined as:

$$I_i = I_{C_i}\left[1 - g(\lambda_i)\right] \tag{3.3}$$

and the estimated EQW therefore transforms into:

$$EQW = \int g(\lambda)\lambda \tag{3.4}$$

3.3 Chromospheric activity measurements

To evaluate the chromospheric activity over the rotation period of a star, Ca II H & K lines are usually used. However, they are sensitive to stellar activity, which can affect the measured radial velocity variations (Karjalainen et al. [2022]). In case of a low signal-to-noise ratio of spectra around the Ca II H & K lines, Ca II triplet lines (8498 Å, 8542 Å and 8662 Å) are often used instead. According to Larson et al. [1993], the 8662 Å line is suitable as a diagnostic of stellar chromospheric activity, because, unlike 8498 Å and 8542 Å lines, it is unaffected by atmospheric water vapor lines near its core.

By observing changes in the flux of monitored spectral lines, we can further analyze the stellar activity and look for periodical changes in their shapes, which leads to proving or denying a potential orbital companion or any stellar oscillations or activity.

4. Software overview

4.1 IRAF

IRAF, short for *Image Reduction and Analysis Facility*, is a collection of software written by the *National Optical Astronomy Observatories* (NOAO) in Tucson, Arizona in 1994, used for the reduction and analysis of astronomical data. The software executes commands via its Command Language (CL) user interface similar to a classic command prompt. Various tasks are structured into packages, which have to be called upon through commands. Custom packages can also be introduced by the user. IRAF works with *.fits* file format, which is commonly used in astronomy.

Although it has been programmed in 1994, the program is still commonly used and it might be considered some of the best software for astronomical data analysis, mostly when it comes to spectrometry. One of the reasons for this could be the ability to easily script tasks, hence automating some of the work. Users can make lists of data files and write scripts to process loads of data at once.

In this thesis, we use the *onedspec* IRAF package to perform the radial velocity correction via *dopcor* task, normalize spectra with the *continuum* task and measure the equivalent widths of spectral lines using the *splot* task with its graphic interface (as shown in the Fig 4.1). First, we zoom into a certain wavelength range and then we mark two continuum points with 'e' and 'e' keystrokes, which sums all the flux between the two positions. We also use it to do a Gaussian fit to estimate a center point of some spectral lines, with which we estimate custom ranges for the line and use the 'e' and 'e' keystrokes to get the flux.

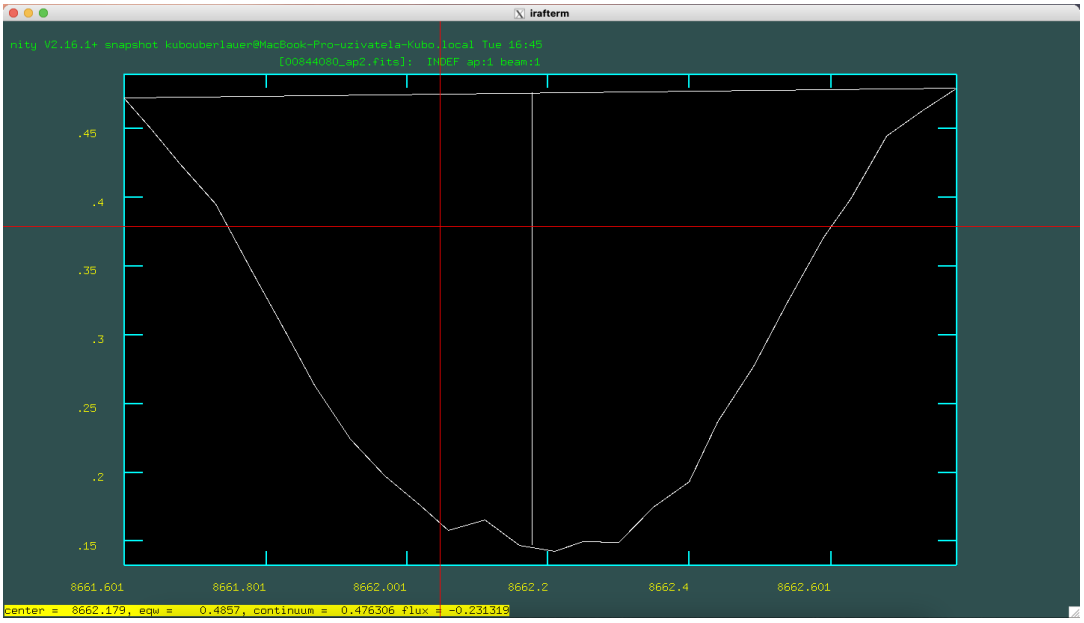

Figure 4.1: The IRAF *splot* interface used to mark two continuum points to measure equivalent width during the HD 187878 measurement.

4.2 Period04

Period04 is a software package designed for time string analysis in astronomical data (Lenz and Breger [2005]). It is composed of 3 different modules: the time string, the fit and the Fourier one (see Fig. 4.2). We use it for finding periodicities in our EQW measurements using the Fourier module. The software uses discrete Fourier transform algorithm to perform Fourier transform of the input data and extract new frequencies from it.

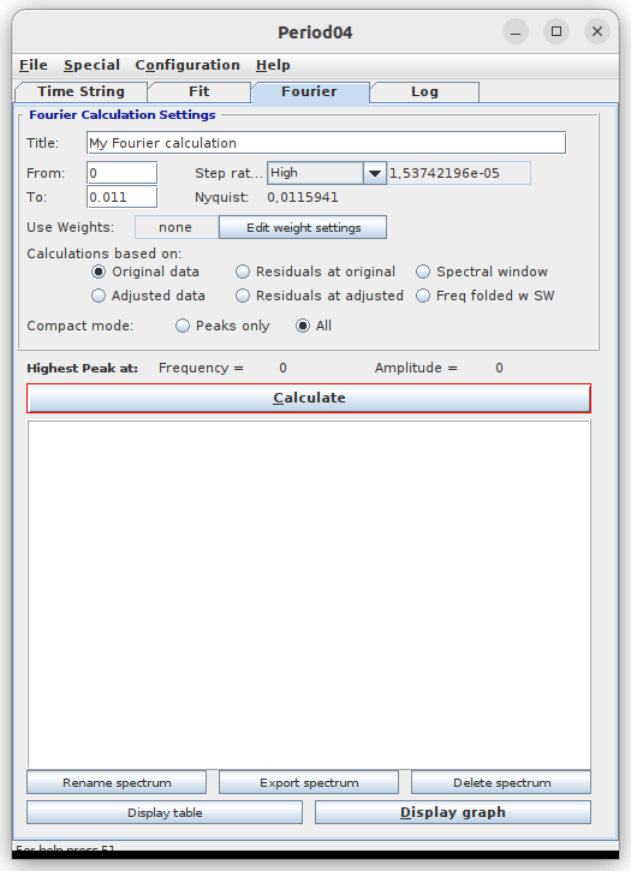

Figure 4.2: Period04 Fourier tab.

A very important variable used in Fourier analysis in Period04 is the Nyquist frequency (also known as folding frequency). In our context, it is the frequency up to which it is reasonable to look for periodicities. In Period04, Nyquist frequency is measures in cycles per day (d^{-1}).

Another important variable is the signal-to-noise ratio. When we find a potentially interesting peak, it is important to test it with the false alarm probability (FAP) over a wide frequency range, meaning the probability of the noise producing a peak with power higher than the one found in the data (Hatzes [2019]). In the Fourier amplitude spectra, we get an estimate of the FAP directly from the signal-to-noise ratio. Optimally, we look for periodicities with signal-to-noise ratio of 3.6 and higher, meaning that the found periodicities are significant and it is reasonable to continue with further Fourier analysis.

After processing the data in Period04, we can view and export graphs. Period04 also logs all actions taken into a *.log* file.

5. Results

We used data from HERMES, a high-resolution fibre-fed echelle spectrograph in the Mercator Telescope at the Observatorio del Roque de Los Muchachos on La Palma in Canary Islands (Raskin et al. [2011]). We used a dedicated automated data reduction pipeline to reduce the data and provide wavelength calibrated spectra with cosmics removed. We performed a barycentric radial velocity correction using the *dopcor* task of IRAF and the program BarCor[1]. The spectra were normalized using the *continuum* task in *onedspec* package.

Having normalized spectra, we can take a closer look at all the desired lines in respective apertures. In both stars, we analyze the same Ca II lines (8662 Å, 8498 Å and 8542 Å), but we use different ranges.

5.1 HD 187878

HD 187878 is a K giant star with a visual magnitude of 7.13 ± 0.01 mag (Høg et al. [2000]). The star's companion was thought to be a brown dwarf, because the minimal mass before the astrometric analysis was bigger than that of a planet. After further data analysis in Karjalainen et al. [2022], we have discovered that the companion is of a stellar mass. We have used the measurements from apertures 2 and 3 of the HERMES spectrograph. The 8662 Å line was located in the aperture 2, for which we had 26 different spectra. The narrow range for calculating equivalent width of this line was set as 8661.6-8662.78 Å and we estimated a wider range as 8661.1-8663.28 Å.

For the lines 8498 Å and 8542 Å, 30 spectra from the aperture 3 were used. The 8498 Å line was set in the range 8497.45-8498.75 Å. The line centers for the 8542 Å line were shifted in wavelength with respect to each other on individual spectra, so it required more work. We decided to use an approximate range of 8541-8543 Å to calculate the average line center by fitting a Gaussian curve. The center had to be established separately for each spectrum. The ranges were also set individually by adding ±0.65 Å to the calculated center point, hence we could not automate the *splot* graphical interface via using lists (as the ranges were different, meaning we had to set *xmin* and *xmax* parameters individually). An overview of the calculated center points and ranges is in Tab. 5.1.

After these measurements, dates and times of observations were attached to each spectrum. These are needed for finding of periodicities in data with Period04. Having the dates of observation included, we used Period04 Fourier tab for the Fourier transform to extract the frequencies. The value of Nyquist frequency is automatically generated when introducing data to the software, so we manually entered a value bit smaller than the generated one, since as mentioned in Section 4.2, the Nyquist frequency set by the program represents the highest frequency for which finding periodicities is reasonable. We analyzed data from all used ranges of each spectral line to calculate the frequencies and looked for the highest signal-to-noise ratio.

[1] https://stelweb.asu.cas.cz/∼marie/Barcor/

spectrum no.	**center [Å]**	***xmin* [Å]**	***xmax* [Å]**
00359427	8542.074	8541.424	8542.724
00361738	8541.927	8541.277	8542.577
00405117	8541.951	8541.301	8542.601
00414083	8542.000	8541.350	8542.650
00417792	8541.992	8541.342	8542.642
00469082	8542.028	8541.378	8542.678
00475589	8541.978	8541.328	8542.628
00481665	8541.986	8541.336	8542.636
00494007	8542.064	8541.414	8542.714
00494945	8542.074	8541.424	8542.724
00554630	8542.088	8541.438	8542.738
00562107	8541.970	8541.320	8542.620
00574722	8542.040	8541.390	8542.690
00579731	8542.043	8541.393	8542.693
00648377	8541.949	8541.299	8542.599
00717965	8541.986	8541.336	8542.636
00782656	8542.017	8541.367	8542.667
00819777	8542.076	8541.426	8542.726
00833686	8542.043	8541.393	8542.693
00844080	8542.087	8541.437	8542.737
00871956	8542.026	8541.376	8542.676
00879407	8542.083	8541.433	8542.733
00886135	8541.966	8541.316	8542.616
00886246	8541.787	8541.137	8542.437
00891739	8542.114	8541.464	8542.764
00893942	8542.139	8541.489	8542.789
00920061	8542.131	8541.481	8542.781
00920065	8542.120	8541.470	8542.770
00926805	8542.107	8541.457	8542.757
00964187	8542.104	8541.454	8542.754

Table 5.1: Calculated center points and the respective ranges of the 8542 Å line for the HD 187878 spectra

range [Å]	$\nu[\mathrm{d}^{-1}]$	$A[\mathrm{km\,s}^{-1}]$	**S/N**
8497.45-8498.75	0.002890	0.006080	2.704170
8542	0.002460	0.008932	3.181100
8661.1-8663.28	0.000246	0.007431	3.371830
8661.6-8662.78	0.000231	0.004239	3.070590

Table 5.2: Frequencies, amplitudes and signal-to-noise ratio from respective ranges of HD 187878 spectra

Since the frequency is in cycles per day (d^{-1}), we obtain the period as an inverse of this value. The frequency with the highest signal-to-noise ratio was found in data from the 8661.1-8663.28 Å range (see Fig 5.1). Inverting the frequency, we get a period of 4065 d with a significance of 3.4σ when using individual lines.

However, in order to have a more robust analysis, we proceeded as following. For each spectrum, we made an average EQW based on the three Ca II lines and four different measurements, and only then we searched for periods using the program Period04. The most significant frequency found was again the one with the period of 4065 d, but this time with a lower significance of 2.8σ.

To summarize, we did not find any significant periods in the EQW measurements. An overview of the Fourier analysis results is in Tab. 5.2. The results of this data analysis were used in Karjalainen et al. [2022].

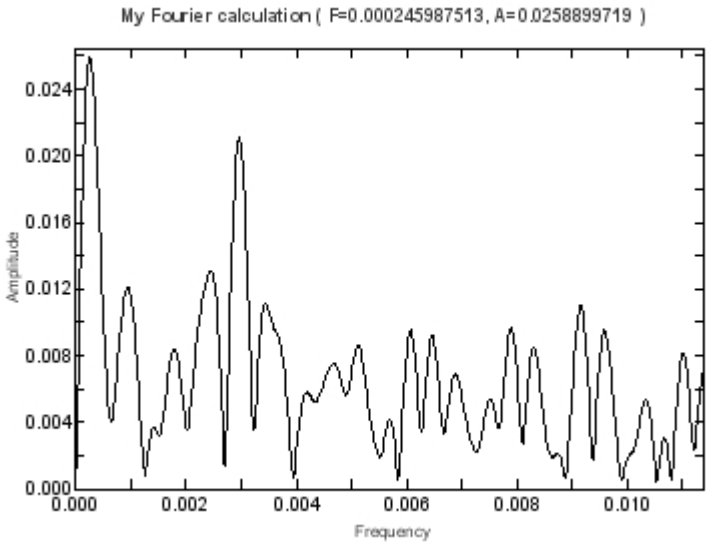

Figure 5.1: Fourier transform of data from the 8661.1-8663.28 Å range of HD 187878 spectra

5.2 KIC 3526061

KIC 3526061 is a K giant star with a visual magnitude of 10.37 ± 0.04 mag (Høg et al. [2000]). From the radial velocity measurements in Karjalainen et al. [2022], we have discovered that the star has a companion that is a brown dwarf of a minimum mass of $18.15\,\mathrm{M_{Jup}}$. As in the previous case, we have used the measurements from apertures 2 and 3 of the HERMES spectrograph. For the 8662 Å line, using 10 spectra from the aperture 2, we have set a narrow range of 8661.55-8662.73 Å and a wider range of 8661-8663.27 Å.

range [Å]	$\nu[\mathrm{d}^{-1}]$	$A[\mathrm{km\,s}^{-1}]$	**S/N**
8497.52-8498.58	0.029738	0.017754	2.129100
8541.63-8542.6	0.008355	0.052658	1.872490
8661.55-8662.73	0.000719	0.047387	2.330700
8661-8663.27	0.000719	0.063807	2.385850

Table 5.3: Frequencies, amplitudes and signal-to-noise ratio from respective ranges for KIC 3526061

For the lines 8498 Å and 8542 Å, we used 10 spectrum measurements from aperture 3. We measured equivalent width of the 8498 Å line in the range 8497.52-8498.58 Å while skipping one of the spectra due to difficult-to-remove sky lines, which have negatively impacted the appearance of the line. The equivalent width of the 8542 Å line was measured in the range 8541.63-8542.6 Å while similarly skipping one of the provided spectra, due to it being shifted towards blue in comparison to other spectra.

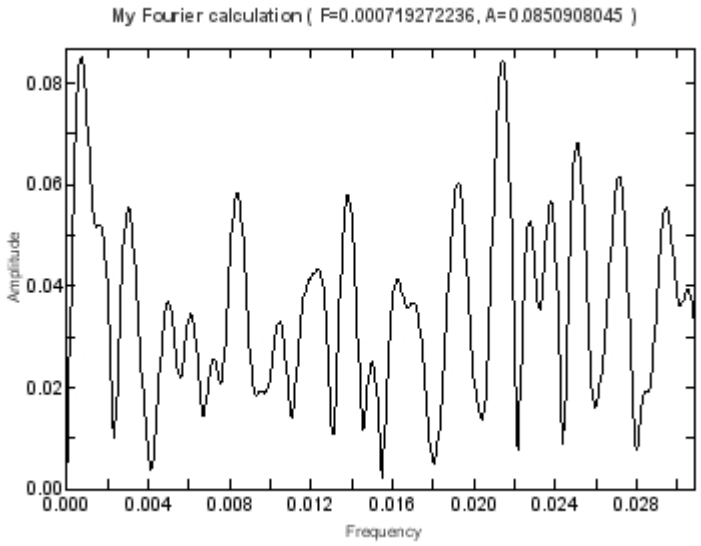

Figure 5.2: Fourier transform of data from the 8661-8663.27 Å range of KIC 3526061 spectra

The process after IRAF measurements was the same as for HD 187878. With the dates and times attached, we input data into Period04, set a marginally smaller Nyquist frequency and look for the periodicities. Unfortunately, none of the analyzed ranges had a signal-to-noise ratio higher than 3.6, meaning we could not find any significant peaks. The cause of this might possibly be the smaller number of recorded spectra available. The graph of the Fourier transform of data from the 8661-8663.27 Å range is depicted in Fig. 5.2. An overview of the Fourier analysis results is in Tab. 5.3. The results of this data analysis were also used in Karjalainen et al. [2022].

Conclusion

In this thesis, we were working with spectra of two K giant stars, HD 187878 and KIC 3526061, obtained by the HERMES echelle spectrograph in the Mercator observatory in Canary Islands (Raskin et al. [2011]). We analyzed data measuring the EQW of the monitored Ca II triplet lines 8492 Å, 8542 Å and 8662 Å in various wavelength ranges using IRAF. We then attached the dates of observations to the files for further analysis and looked for periodicities using Fourier transform analysis via Period04, which also calculated the signal-to-noise ratio of all frequencies found in data.

In general, chromospheric activity is monitored and measured because it is an indicator of stellar activity. Both the stellar activity and oscillations produce asymmetries of stellar spectral lines. A transiting planet causes such asymmetries too. Chromospheric activity is usually measured for stars hosting planet candidates to rule out that a candidate planet signal would in fact come from stellar activity or oscillations. With the precise enough data, one can investigate and eventually find reasons behind observed changes in spectral line asymmetries.

For HD 187878, the period with the highest signal-to-noise ratio was found in the wavelength range of 8661.1-8662.28 Å and it is that of 4065 d. However, the significance of this period is not high enough. In Karjalainen et al. [2022], a stellar companion of HD 187878 was found using the radial velocity method. Its orbital period was calculated as 1452.3 d, which is smaller than the period we found in our analysis of the chromospheric activity. Clearly, the period found in our analysis and the orbital period of the companion are not related. Besides, the period of 4065 d is not significant. In principle, one could, however, take more measurements with higher spectral resolution and higher signal-to-noise ratio to see whether this period is real or not. Also, a possible origin of this period remains unknown.

For KIC 3526061, we did not find any significant peaks in the analysis of EQW measurements. The highest signal-to-noise ratio in the observed data was found in the wider range of the 8662 Å Calcium triplet line, but it is not of high significance. The possible explanation could be that our spectra had too low signal-to-noise ratio and resolution to be able to extract any reasonable signal from the EQW measurements, and that we had too little spectra available. Also, the spectrograph stability plays a significant role. As presented in Karjalainen et al. [2022], a brown dwarf companion with the orbital period of 3552 d was found orbiting KIC 3526061. None of the extracted periods in the analysis of EQW measurements agrees with the orbital period of the companion, and also all the extracted periods are insignificant.

The outcome of this thesis demonstrates the difficulty of finding periodicities in data with not high enough spectral resolution and data observed by not stable enough spectrographs. However, this is in no means a proof that these periodicities caused by stellar oscillations or activity do not exist in data, but we do not have tools sensitive enough to detect them.

Bibliography

Arnold Hanslmeier. *The Chaotic Solar Cycle*. Springer Singapore, 2020. doi: 10.1007/978-981-15-9821-0.

A P Hatzes. *The Doppler Method for the Detection of Exoplanets*. 2514-3433. IOP Publishing, 2019. ISBN 978-0-7503-1689-7. doi: 10.1088/2514-3433/ab46a3. URL `https://dx.doi.org/10.1088/2514-3433/ab46a3`.

E. Høg, C. Fabricius, V. V. Makarov, S. Urban, T. Corbin, G. Wycoff, U. Bastian, P. Schwekendiek, and A. Wicenec. The Tycho-2 catalogue of the 2.5 million brightest stars. *Astronomy & Astrophysics*, 355:L27–L30, March 2000.

Marie Karjalainen, Raine Karjalainen, Artie P. Hatzes, Holger Lehmann, Pierre Kervella, Saskia Hekker, Hans Van Winckel, Jakub Üeberlauer, Michaela Vítková, Marek Skarka, Petr Kabáth, Saskia Prins, Andrew Tkachenko, William D. Cochran, and Alain Jorissen. Companions to Kepler giant stars: A long-period eccentric sub-stellar companion to KIC 3526061 and a stellar companion to HD 187878. *Astronomy & Astrophysics*, 668:A26, December 2022. doi: 10.1051/0004-6361/202244501.

Ana M. Larson, Alan W. Irwin, Stephenson L. S. Yang, Cherie Goodenough, Gordon A. H. Walker, Andrew R. Walker, and David A. Bohlender. A CA II lambda-8662 Index of Chromospheric Activity: The Case of 61 Cygni A. *Publications of the Astronomical Society of the Pacific*, 105:332, April 1993. doi: 10.1086/133159.

P. Lenz and M. Breger. Period04 User Guide. *Communications in Asteroseismology*, 146:53–136, June 2005. doi: 10.1553/cia146s53.

Michel Mayor and Didier Queloz. A Jupiter-mass companion to a solar-type star. *Nature*, 378(6555):355–359, November 1995. doi: 10.1038/378355a0.

G. Raskin, H. van Winckel, H. Hensberge, A. Jorissen, H. Lehmann, C. Waelkens, G. Avila, J. P. de Cuyper, P. Degroote, R. Dubosson, L. Dumortier, Y. Frémat, U. Laux, B. Michaud, J. Morren, J. Perez Padilla, W. Pessemier, S. Prins, K. Smolders, S. van Eck, and J. Winkler. HERMES: a high-resolution fibre-fed spectrograph for the Mercator telescope. *Astronomy & Astrophysics*, 526:A69, February 2011. doi: 10.1051/0004-6361/201015435.

Peter B. Stetson and Elena Pancino. DAOSPEC: An Automatic Code for Measuring Equivalent Widths in High-Resolution Stellar Spectra. *Publications of the Astronomical Society of the Pacific*, 120(874):1332, December 2008. doi: 10.1086/596126.

Alexander Wolszczan. Confirmation of Earth-Mass Planets Orbiting the Millisecond Pulsar PSR B1257+12. *Science*, 264(5158):538–542, April 1994. doi: 10.1126/science.264.5158.538.

List of Figures

1.1 The Hertzsprung-Russell diagram. ESO 5
1.2 Heat transfer of stars depending on their mass. Wikipedia 7

2.1 Illustration of changes of a star's brightness during a planetary transit. ESA 10
2.2 A visual depiction of the Doppler effect caused by the movement of a star around the system's barycenter. The Royal Swedish Academy of Science 12

3.1 A continuous, an emission and an absorption spectrum. University of Rochester 13
3.2 The black-body radiation model. Encyclopaedia Britannica. . . . 14
3.3 Visual representation of the EQW definition. Stetson and Pancino [2008] 15

4.1 The IRAF *splot* interface used to mark two continuum points to measure equivalent width during the HD 187878 measurement. . . 17
4.2 Period04 Fourier tab. 18

5.1 Fourier transform of data from the 8661.1-8663.28 Å range of HD 187878 spectra 21
5.2 Fourier transform of data from the 8661-8663.27 Å range of KIC 3526061 spectra 22

List of Tables

5.1 Calculated center points and the respective ranges of the 8542 Å line for the HD 187878 spectra 20
5.2 Frequencies, amplitudes and signal-to-noise ratio from respective ranges of HD 187878 spectra 20
5.3 Frequencies, amplitudes and signal-to-noise ratio from respective ranges for KIC 3526061 21